Pergamon

Int. J. Heat Mass Transfer. Vol. 38, No. 5, pp. 909–919, 1995

0017-9310/95 $9.50+0.00

0017-9310(94)00195-2

Vapor bubble growth in heterogeneous boiling—I. Formulation

RENWEI MEI

Department of Aerospace Engineering, Mechanics & Engineering Science, University of Florida, Gainesville, FL 32611, U.S.A.

and

WENCHIN CHEN and JAMES F. KLAUSNER

Department of Mechanical Engineering, University of Florida, Gainesville, FL 32611, U.S.A.

(*Received* 13 *December* 1993 *and in final form* 17 *June* 1994)

Abstract—A numerical analysis is carried out to study bubble growth in saturated heterogeneous boiling. The bubble growth is determined by considering the simultaneous energy transfer among the vapor bubble, liquid microlayer, and heater. Finite difference solutions for the temperature fields in the microlayer and heater are obtained on expanding coordinates as the bubble grows. The parameters characterizing the bubble shape and microlayer wedge angle are determined by matching the existing experimental data. The predicted bubble growth rate compares very well with the reported experimental data over a wide range of conditions.

1. INTRODUCTION

1.1. *Background*

Over the past four decades, the rate of vapor bubble growth in heterogeneous boiling systems has been the subject of numerous experimental and theoretical investigations due to its governing influence on heat transfer. A number of theoretical investigations on bubble growth rate have been conducted for uniformly superheated liquids [1–4] and nonuniformly superheated liquids [5–10]; various closed-form expressions for the growth rate have been proposed. Extensive experimental data exist which demonstrate that such expressions do not accurately predict the vapor bubble growth rate in heterogeneous boiling. In particular, the inadequacy of such expressions have been clearly shown in Cole and Shulman [11] and Van Stralen *et al.* [12] for high Jacob number, Staniszewski [13] and Akiyama *et al.* [14] for low Jacob number, and Keshock and Siegel [15] for low gravity.

Labunstov [16] recognized that the majority of heat transfer to a growing vapor bubble occurs in a liquid microlayer which resides beneath its base; he derived a vapor bubble growth expression by assuming a constant wall temperature. Cooper [17] also developed a microlayer bubble growth model by assuming a constant wall temperature. Dzakowic and Frost [18] calculated the vapor bubble growth rate using a constant wall temperature evaporating microlayer model in which the transient microlayer thermal field is accounted for. Srinivas and Kumar [19] proposed a microlayer bubble growth model which accounts for the bubble shape as well as natural convection and assumes a constant wall temperature. However, these models do not agree well with available experimental data [11–15]. Cooper and Vijuk [20] and Van Stralen *et al.* [21] have considered the heat transfer to a growing vapor bubble from both the microlayer and the liquid surrounding the vapor dome. Asymptotic expressions for the vapor bubble growth rate were derived by combining Rayleigh's solution for the initial stage of growth with the heat transfer controlled solution. The growth model of Van Stralen *et al.* [21] appears to agree better with the high Jacob number data than that of Cooper and Vijuk [20]. However, its usefulness is limited due to the required specification of a dimensionless bubble growth parameter for which little guidance was provided on how it should be calculated. Fyodorov and Klimenko [22] recently proposed a microlayer bubble growth rate model in which spatial variations in the wall temperature were included, but the temporal variations were ignored. Their growth rate model predicts that the bubble radius is proportional to the square root of time, $t^{1/2}$. However, the data of Akiyama *et al.* [14] clearly demonstrate that the exponent on t can be as small as 1/5 at very low Jacob number.

In their model for predicting the growth and detachment of a vapor bubble attached to a heating surface, Lee and Nydahl [23] incorporated the effect of hydrodynamics surrounding the dome of the growing bubble. They assumed a constant wall temperature, modelled the bubble as consisting of a wedge-shaped microlayer and a hemisphere, and carried out detailed numerical computations for the momentum and

NOMENCLATURE

A area of microlayer wedge
c bubble shape parameter $[R_b(t)/R(t)]$; empirically determined
c_1 microlayer wedge angle parameter; empirically determined
c_{pl} liquid specific heat
$f(c)$ bubble volume factor; given by equation (3)
Fo Fourier number
h_{fg} latent heat of vaporization
H solid heater thickness
k_l and k_s liquid and solid thermal conductivity
Ja Jacob number
$L(r)$ local microlayer thickness
Pr_l liquid Prandtl number
q'' and q''' heat supply from the bottom of the heater and within the heater
r radial coordinate
$\bar{r}$ dimensionless radial coordinate scaled by microlayer radius, $r/R_b(t)$
$R(t)$ actual bubble radius
$\dot{R}(t)$ actual bubble growth rate
$R_b(t)$ radius of the liquid microlayer underneath the bubble
$R_c(t)$ bubble radius assuming a constant wall temperature
$\bar{R}$ dimensionless bubble growth rate
S_r and S_z constants used in the grid stretching
t time
t_d vapor bubble departure time scale
t_0 initial time for the computation
T_l and T_s liquid and solid temperature
T_{sat} saturated temperature
z coordinate in the direction normal to the heating surface
$\bar{z}_l$ and $\bar{z}_s$ dimensionless coordinates in the liquid microlayer and solid heater.

Greek symbols
α liquid-to-solid thermal diffusivity ratio, α_l/α_s
α_l and α_s liquid and solid thermal diffusivity
β a constant for bubble radius at constant wall temperature
δ_{th} thermal layer thickness of the bulk liquid
ΔT_{sat0} initial superheat at incipience
ϕ microlayer wedge angle [rad]
η and ζ computational coordinates
κ liquid-to-solid thermal conductivity ratio, k_l/k_s
ν_l liquid kinematic viscosity
ρ_l and ρ_v liquid and vapor density
θ_l and θ_s dimensionless temperature of liquid and solid
σ transformed time coordinate, $\tau^{1/2}$
$\Delta\sigma$ "time step" in the transformed time coordinate
τ dimensionless time, t/t_d
τ_0 initial time (dimensionless) at the beginning of the computation.

energy equations for the liquid phase surrounding the vapor bubble. However, their predictions for the bubble growth rate and the detachment radius are not satisfactory when compared against experimental data.

Despite the importance of predicting the bubble growth rate in heterogeneous boiling and continuous research efforts covering the subject, no satisfactory theory has been formulated to cover a wide range of conditions. In the recent works for predicting the vapor bubble detachment diameter for pool boiling [24] and that for flow boiling [25], a successful model was developed based on first principles of mechanics. The predictions for the detachment radius agree quite well with the data over a wide range of conditions; however, the agreement was obtained only after using the actual bubble growth rate reported for each experiment. Clearly, without a reliable, physically sound bubble growth rate model the utility of the bubble detachment models [24, 25] is limited.

1.2. *Physical features of the bubble growth process considered in the present analysis*

In the previous works for predicting the growth rate of a bubble attached to a heating surface, the simultaneous spatial and temporal changes of the heating surface temperature were not considered. However, the temperature distribution in the neighborhood of a heater wall has long been believed by Westwater [26] to be important to the mechanics of bubble growth. In reality, the growth of a bubble requires a certain amount of energy from the heating surface to vaporize the surrounding liquid. In saturated boiling, this energy must come from the microlayer which resides beneath the base of the bubble and in turn withdraws energy from the solid heater [27]. Typically, the growth and departure of a vapor bubble involve a very short period [28]. Although energy is continuously supplied to the solid, the time scale required for the solid to adjust its temperature into a uniform distribution for most boiling systems

is much longer than the bubble departure time. Consequently, the local solid temperature directly beneath the microlayer will decrease, both in space and in time, because the local rate of energy removal due to the bubble growth is typically much larger than that added. The rapid decrease of the heating surface temperature directly beneath a growing vapor bubble has been experimentally demonstrated by Moore and Mesler [27] and Hospeti and Mesler [28]. As the local solid wall temperature decreases with time during the bubble growth period, the temperature gradient across the microlayer is reduced and in turn directly reduces the rate of energy transferred to the bubble. Therefore, the actual bubble growth rate should be smaller than that predicted by assuming a constant wall temperature. This prognosis is in qualitative agreement with the existing data which show that the growth rate $R(t)$ is less than or equal to $\beta t^{1/2}$ in which β is a constant.

In this paper, the bubble growth process is considered to be controlled by the simultaneous unsteady energy transfer process among three phases: the vapor bubble, the liquid microlayer and the solid heater. The bubble is assumed to have a uniform temperature at saturated conditions, T_{sat0}; the liquid microlayer is assumed to be very thin; and the temperature field in the solid is assumed to be axisymmetric with respect to (wrt) the axis normal to the heating surface and drawn through the center of the bubble. In Section 2.1, pertinent assumptions are made and the equations, the boundary conditions and the initial conditions governing the unsteady energy transfer from the solid layer through the microlayer to the bubble are presented. In Section 2.2, non-dimensionalization and coordinate transformations are presented which lead to necessary simplifications of the governing equations. The solution procedure for the microlayer and solid temperature fields and the bubble radius is also described. The parameters characterizing the bubble shape and the microlayer wedge angle during the growth are determined by matching the predicted growth rate with the existing experimental data. The predicted bubble growth rate is compared with the available experimental data over a wide range of conditions in Section 3.2; very good agreement is obtained. Notably, it is found that the Prandtl number has little or no effect on the bubble growth rate for the experimental conditions considered. To assist the basic understanding of bubble growth in heterogeneous boiling, the results of a systematic study considering the dependence of the bubble growth rate and the thermal fields of the liquid microlayer and the solid heater on the dimensionless parameters are reported in Part II of this study [29].

2. FORMULATION

2.1. *Assumptions, governing equations, and boundary and initial conditions*

2.1.1. *On the vapor bubble.* A rigorous description of the vapor bubble growth and heat transfer processes among three phases requires a complete account for the hydrodynamics around the rapidly growing bubble in addition to the complex thermal energy transfer. The most difficult part, perhaps, is the exact determination of the bubble shape which is a moving interface between the vapor and liquid. The numerical analysis by Lee and Nydahl [23] still relied on an assumed shape for the bubble, although the hydrodynamics based on the assumed bubble shape is properly accounted for. The discussion in the Introduction suggests that the thermal coupling between the liquid microlayer and the solid heater is perhaps more important than hydrodynamics. Therefore, in order to simplify the problem, the hydrodynamics of the liquid motion induced by the growing bubble is not pursued in this analysis. The determination of the bubble shape thus relies on empirical evidence. Furthermore, it is assumed that energy transfer to the bubble occurs only through the microlayer, and energy transfer to the bubble dome is small. Thus, the current analysis is only applicable to *saturated boiling*.

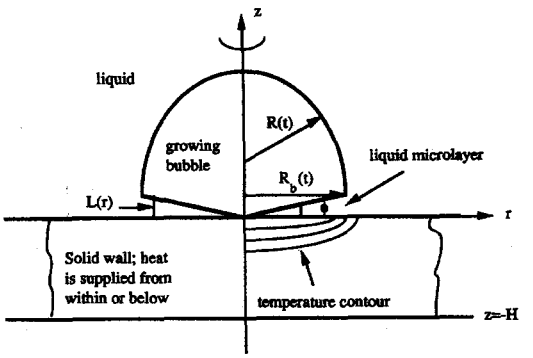

Fig. 1. Sketch for the growing bubble, microlayer and the heating solid.

In this study, the liquid microlayer between the vapor bubble and the solid heating surface is assumed to have a simple wedge shape with an angle $\phi \ll 1$. In this paper, ϕ is measured in radians. The interferometry measurements of Koffman and Plesset [30] demonstrate that a wedge shaped microlayer is a good assumption. There exists ample experimental evidence [12, 14, 27] suggesting that, as the bubble grows, the dome has approximately a spherical shape with a radius $R(t)$, as shown in Fig. 1. Using cylindrical coordinates, the local microlayer thickness is denoted by $L(r)$. The radius of the wedge-shaped interface is denoted by $R_b(t)$ which is typically not equal to $R(t)$. Let

$$c = R_b(t)/R(t) \tag{1}$$

and the vapor bubble volume $V_b(t)$ can be expressed approximately as

$$V_b(t) = \frac{4\pi}{3} R^3(t) f(c) \tag{2}$$

with

$$f(c) \approx 1-\tfrac{3}{4}[1-\sqrt{(1-c^2)}]^2+\tfrac{1}{4}[1-\sqrt{(1-c^2)}]^3$$

$$\text{for } \phi \ll 1. \tag{3}$$

In the limit $c \to 1$, the bubble is a hemisphere and $V_b(t) \to (2\pi/3)R^3(t)$. In the limit $c \to 0$, the bubble approaches a sphere and $V_b(t) \to (4\pi/3)R^3(t)$. The dependence of c on other parameters will be determined from the reported measurements of the bubble shape under various conditions. In this study, c is assumed to be independent of time for simplicity.

An energy balance at the liquid–vapor interface for the growing bubble depicted in Fig. 1 is described as

$$\rho_v h_{fg} f(c) 4\pi R^2 \frac{dR}{dt} = \int_A -k_l \left(\frac{\partial T_l}{\partial z}\right)_{z=L(r)} dA$$

$$\text{for } \phi \ll 1 \tag{4}$$

where ρ_v is the vapor density, h_{fg} the latent heat, k_l the liquid thermal conductivity, T_l the liquid temperature and A the area of the wedge. With axisymmetry and $\phi \ll 1$, $dA = 2\pi r\,dr$ and $A = \pi R_b^2(t)$ at a given instant. Equation (4) simply states that the energy conducted from the liquid to the bubble through the microlayer is used to vaporize the surrounding liquid and thus expand the bubble. The initial condition for $R(t)$ will be discussed later.

2.1.2. *On the microlayer.* The microlayer is assumed to be a wedge centered at $r = 0$ with local thickness $L(r)$. Because the hydrodynamics are not considered, the microlayer wedge angle ϕ cannot be determined as part of the solution. In Cooper and Lloyd [31], the angle ϕ was related to the viscous diffusion length of the liquid as $R_b(t)\tan\phi = c_1\sqrt{(\nu_l t)}$ in which ν_l is the kinematic viscosity of the liquid. Hence for small ϕ, one has

$$\phi = \frac{c_1\sqrt{(\nu_l t)}}{R_b(t)} = \frac{c_1\sqrt{(\nu_l t)}}{cR(t)}. \tag{5}$$

Cooper and Lloyd [31] estimated c_1 to be within 0.3–1.0 for the conditions under their consideration. It is postulated here that the behavior of ϕ is insensitive to whether or not the wall temperature is constant. Thus the above form of equation (5) for ϕ is adopted. The constant c_1 will be determined from matching the predicted growth rate $R(t)$ with the experimentally measured growth rate. The two dimensionless constants, c and c_1, constitute the only empiricism of the present analysis. They arise because the hydrodynamics around the bubble are not taken into account in the analysis which follows.

For both the microlayer and the solid, the temperature fields are assumed to be axisymmetric. The energy balance for the liquid within the microlayer is

$$\frac{\partial T_l}{\partial t} = \alpha_l\left[\frac{1}{r}\frac{\partial}{\partial r}\left(r\frac{\partial T_l}{\partial r}\right)+\frac{\partial^2 T_l}{\partial z^2}\right]$$

$$\text{for } 0 \leqslant r \leqslant R_b(t) \quad 0 \leqslant z \leqslant L(r) \tag{6}$$

where α_l is the liquid thermal diffusivity. The boundary conditions are given as follows:

$$T_l = T_{sat} \quad \text{at } z = L(r) \tag{7}$$

$$T_l = T_s \text{ and } k_l\frac{\partial T_l}{\partial z} = k_s\frac{\partial T_s}{\partial z} \quad \text{at } z = 0 \tag{8}$$

$$\frac{\partial T_l}{\partial r} = 0 \quad \text{at } r = 0 \tag{9}$$

$$\frac{\partial T_l}{\partial r} = 0 \quad \text{at } r = R_b(t). \tag{10}$$

In the above, T_s is the solid temperature. Equations (8) simply ensure the continuity of the temperature and heat flux on the liquid–solid interface. Equation (10) is only an approximation in which radial heat conduction at the edge of the microlayer is neglected. Equation (9) guarantees that T_l is finite as $r \to 0$. The initial condition for T_l is discussed later.

2.1.3. *On the solid heater.* The energy equation for the solid is

$$\frac{\partial T_s}{\partial t} = \alpha_s\left[\frac{1}{r}\frac{\partial}{\partial r}\left(r\frac{\partial T_s}{\partial r}\right)+\frac{\partial^2 T_s}{\partial z^2}\right]+\frac{\alpha_s}{k_s}q'''$$

$$\text{for } 0 \leqslant r < \infty \quad -H < z < 0 \tag{11}$$

where α_s and k_s are the thermal diffusivity and conductivity of the solid, and q''' is the volumetric heating and H is the thickness of the heater. The boundary conditions are

$$\frac{\partial T_s}{\partial r} = 0 \quad \text{at } r = 0 \text{ and } r \to \infty \tag{12}$$

$$\frac{\partial T_s}{\partial z} = -q''/k_s \quad \text{at } z = -H \tag{13}$$

$$T_l = T_s \text{ and } k_l\frac{\partial T_l}{\partial z} = k_s\frac{\partial T_s}{\partial z} \quad \text{at } z = 0 \quad 0 \leqslant r \leqslant R_b(t) \tag{14}$$

$$T_l = T_s \text{ and } \frac{\partial T_s}{\partial z} = 0 \quad \text{at } z = 0 \quad r \geqslant R_b(t). \tag{15}$$

In the above, two possible mechanisms for heat supply are incorporated: a heat supply on the lower surface at $z = -H$, q'', or a volumetric heat supply (on average) within the solid layer, q'''. For $r > R_b(t)$ at $z = 0$, the heat transfer due to natural convection of the liquid is neglected. Whether or not the heat removal from the solid due to natural convection is included, it has virtually no influence on the solution because it is so small compared with latent heat removed due to bubble growth. The condition at $r \to \infty$ reflects the uniformity of the temperature far away from the bubble. Because of the continuous energy supply, it is not quite correct to specify, for all times, $T_s = T_{sat} + \Delta T_{sat0}$ as $r \to \infty$ in which ΔT_{sat0} is the initial superheat at incipience. If there exists strong thermal interaction among adjacent nucleation sites, as might occur in the coalesced bubble regime, the present analysis needs to

be modified. Hence, the present analysis is restricted, strictly speaking, to the isolated bubble regime.

2.1.4. *On the initial conditions.* It must be noted that the above formulation requires a well-established microlayer at the beginning of the solution. This implies that the solution must start at some finite but small time $t_0 \ll t_d$ in which t_d is the departure time of the bubble and is the time scale of interest for the present problem. It is assumed here that at $t = t_0$ the microlayer has formed and the bubble has a radius R_0. But, since R_0 is small, the bubble has withdrawn little energy from the solid at $t = t_0$. Thus, the solid temperature T_s is practically constant everywhere:

$$T_s = T_{sat} + \Delta T_{sat0} \quad \text{at } t = t_0 \ll t_d. \tag{16}$$

This assumption is justified because the initial stage of the growth is governed by hydrodynamic considerations as is the case for Rayleigh's solution. The present study focuses on the coupling of the solid temperature with that of the liquid and the rate of bubble growth. However, this coupling becomes important only after a significant amount of energy is transferred from the solid to the bubble through the microlayer. Therefore, a reasonable initial condition for T_l is

$$T_l(t = t_0, r \leqslant R_0, z) = T_{sat} + \Delta T_{sat0}\left[1 - \frac{z}{L(r)}\right] \quad \text{at } t = t_0 \ll t_d. \tag{17}$$

Consistent with equations (16) and (17), the initial bubble radius at $t = t_0$ can be obtained by assuming a constant wall temperature. This is appropriate because the solid temperature is not affected yet by the growth of the bubble at very small t_0. Integrating equation (4) by assuming a time independent $\partial T_l/\partial z$, one obtains

$$R_c(t) = \frac{c^2}{f(c)} \frac{Ja}{c_1 Pr_l^{1/2}} (\alpha_l t)^{1/2} \tag{18}$$

for the growth rate with a constant wall temperature. In the above

$$Ja = \frac{\rho_l c_{pl} \Delta T_{sat0}}{\rho_v h_{fg}} \tag{19}$$

and

$$Pr_l = \frac{\nu_l}{\alpha_l} \tag{20}$$

are the Jacob number and Prandtl number, respectively, and c_{pl} is the specific heat of the liquid. Hence R_0 can be found as $R_0 = R_c(t_0)$. In equation (18), the relation between ϕ and $R(t)$ given by equation (5) has been used. Equations (16)–(18) complete the specification of the initial conditions. Although the actual initial growth is governed by hydrodynamics, this assumed initial radius has little effect on the later growth as long as $t_0 \ll t_d$. It is noted that the liquid Prandtl number Pr_l results from Cooper and Lloyd's model for the microlayer wedge angle ϕ given by equation (5), and, using equation (18), ϕ may be expressed as

$$\phi = \frac{f(c) c_1^2 Pr_l}{c^3 Ja}. \tag{5a}$$

2.2. *Non-dimensionalization and coordinate transformation*

2.2.1. *Non-dimensionalization and further simplifications.* To gain an understanding of the important physics and to efficiently solve the energy equations, the following dimensionless variables are introduced:

$$\tau = t/t_d \quad \bar{r} = r/R_b(t) \quad \bar{z}_l = z/L(r) \quad \bar{z}_s = z/H$$

$$\bar{R}(\tau) = \frac{R(t)}{R_c(t_d)} \quad \theta_l = (T_l - T_{sat})/\Delta T_{sat0}$$

$$\theta_s = (T_s - T_{sat})/\Delta T_{sat0} \tag{21}$$

where t_d is the bubble departure time scale. An accurate determination of t_d is not necessary because only the time scale is relevant. The length scale in the z-direction for the solid is the thickness of the heater. However, this is not the correct length scale if H is very large or the solid conductivity is very small. Thus another transformation is expected for $\bar{z}_s$ in carrying out the computation. The utilization of H is sufficient for the purpose of dimensional analysis.

Upon substitution of equation (21) into equation (4), the normalized bubble growth rate is governed by

$$\frac{d\bar{R}^2(\tau)}{d\tau} = -\int_0^1 \left(\frac{\partial \theta_l}{\partial \bar{z}_l}\right)_{\bar{z}_l = 1} d\bar{r}. \tag{22}$$

For constant wall temperature, the right-hand-side (RHS) of equation (22) is unity and $\bar{R}(\tau) = \tau^{1/2}$. Hence, any mechanism that causes $|(\partial\theta_l/\partial\bar{z}_l)|_{\bar{z}_l = 1}$ to decrease with time will yield a growth rate $\bar{R}(\tau) < \tau^{1/2}$.

Substituting the above dimensionless variables into the governing equations, one obtains for the microlayer

$$\frac{\partial \theta_l}{\partial \tau} - \frac{t_d \dot{R}_b}{R_b} \bar{r} \frac{\partial \theta_l}{\partial \bar{r}} = \frac{\alpha_l t_d}{R_b^2(\tau)} \frac{1}{\bar{r}} \frac{\partial}{\partial \bar{r}}\left(\bar{r} \frac{\partial \theta_l}{\partial \bar{r}}\right) - \frac{\alpha_l t_d L'(\bar{r})}{R_b(\tau) L(\bar{r})} \frac{\bar{z}_l}{\bar{r}} \frac{\partial \theta_l}{\partial \bar{z}_l} + \frac{\alpha_l t_d}{L^2(\bar{r})} \frac{\partial^2 \theta_l}{\partial \bar{z}_l^2} \tag{23}$$

for $0 \leqslant \bar{r} \leqslant 1$, $0 \leqslant \bar{z}_l \leqslant 1$. In the above

$$L'(r) = \frac{dL}{dr} = \phi \ll 1 \quad \dot{R}_b = \frac{dR_b}{dt}$$

and

$$L(\bar{r}) \leqslant L(1) = \phi R_b(\tau) \ll R_b(\tau).$$

For very small ϕ, the RHS of equation (23) reduces to

$$\frac{\alpha t_d}{L^2(\bar{r})}\left\{\phi^2 \frac{\partial}{\partial \bar{r}}\left(\bar{r} \frac{\partial \theta_l}{\partial \bar{r}}\right) - \phi^2 \frac{\bar{z}_l}{\bar{r}} \frac{\partial \theta_l}{\partial \bar{z}_l} + \frac{\partial^2 \theta_l}{\partial \bar{z}_l^2}\right\} \sim \frac{\alpha_l t_d}{L^2(\bar{r})} \frac{\partial^2 \theta_l}{\partial \bar{z}_l^2}$$

and consequently equation (23) becomes, to the leading order for small ϕ,

$$\frac{\partial\theta_l}{\partial\tau}-\frac{\bar{R}'(\tau)}{\bar{R}(\tau)}\bar{r}\frac{\partial\theta_l}{\partial\bar{r}}=\frac{1}{c_1^2Pr_l}\frac{1}{\bar{r}^2\bar{R}^2(\tau)}\frac{\partial^2\theta_l}{\partial\bar{z}_l^2}$$

$$\text{for } 0\leqslant\bar{r}\leqslant 1\quad 0\leqslant\bar{z}_l\leqslant 1 \tag{24}$$

where the prime denotes the time derivative wrt τ. If $c_1^2Pr_l\ll 1$, the conduction term dominates and a quasi-steady heat conduction problem results. Only for some cases, such as low Jacob number boiling, it is possible that $c_1^2Pr_l\ll 1$. Hence all three terms on equation (24) must be retained for numerical accuracy.

It is noted that since the second order derivative wrt $\bar{r}$ disappears following the foregoing scaling analysis, only one boundary condition in the $\bar{r}$-direction is required. Because $\bar{R}'(\tau)>0$, the first order derivative wrt $\bar{r}$ acts as a convection term with a negative speed in the $\bar{r}$-direction. Thus the condition at $\bar{r}=0$ given by equation (9) is dropped. The advantage of solving equation (24) over equation (23) is that equation (24) is parabolic, instead of elliptic, and marching from $\bar{r}=1$ to $\bar{r}=0$ for equation (24) is relatively simple.

For the solid layer, the energy equation in dimensionless form is

$$\frac{\partial\theta_s}{\partial\tau}-\frac{\bar{R}'(\tau)}{\bar{R}(\tau)}\bar{r}\frac{\partial\theta_s}{\partial\bar{r}}=\frac{\alpha_s t_d}{R_b^2(\tau)}\frac{1}{\bar{r}}\frac{\partial}{\partial\bar{r}}\left(\bar{r}\frac{\partial\theta_s}{\partial\bar{r}}\right)$$

$$+\frac{\alpha_s t_d}{H^2}\frac{\partial^2\theta_s}{\partial\bar{z}_s^2}+\frac{\alpha_s t_d q'''}{k_s\Delta T_{sat0}} \tag{25}$$

for $0\leqslant\bar{r}<\infty$, $-1\leqslant\bar{z}_s\leqslant 0$. For the first term on the RHS of equation (25), the ratio $(R_b(\tau)/H)^2$ is small at the early stage of growth but can be large at a later time if a thin heater is used. Thus unlike the liquid microlayer case, both the derivatives wrt $\bar{r}$ and $\bar{z}_s$ are important in equation (25). Using equations (1), (18) and (21), equation (25) can be expressed as

$$\frac{\partial\theta_s}{\partial\tau}-\frac{\bar{R}'(\tau)}{\bar{R}(\tau)}\bar{r}\frac{\partial\theta_s}{\partial\bar{r}}=\frac{1}{\alpha}\frac{f^2(c)c_1^2Pr_l}{c^6Ja^2}\frac{1}{\bar{R}^2(\tau)}\frac{1}{\bar{r}}\frac{\partial}{\partial\bar{r}}\left(\bar{r}\frac{\partial\theta_s}{\partial\bar{r}}\right)$$

$$+Fo\frac{\partial^2\theta_s}{\partial\bar{z}_s^2}+\frac{\alpha_s t_d q'''}{k_s\Delta T_{sat0}} \tag{26}$$

where

$$Fo=\frac{\alpha_s t_d}{H^2} \tag{27}$$

is the solid Fourier number. The last term in equation (26) is usually insignificant during the early stages of growth. In all the data analyzed, when neglected, the last term causes at most 10% error for $\bar{R}(\tau)$. Although this term is kept in the computation to obtain better values for c_1, no particular attention will be given to its effect on the growth rate.

It is emphasized here that the introduction of the bubble departure time scale, t_d, in the *computation* of the growth rate is an artifact. The growth rate $R(t)$ in dimensional form is independent of t_d. However, t_d is a useful quantity to characterize the effective thickness of the heater in defining Fo and to scale the growth time. If t_d is quite small so that $Fo\ll 1$, the heater is considered to be very thick and the temperature at the bottom of the heater is not affected by the time the bubble departs. If $Fo\sim O(1)$ or larger, the temperature on the bottom of the heater will be influenced by the bubble growth on a time scale of t_d. The thermal interaction between the bubble and the heater, which determines the bubble growth rate, thus depends strongly on Fo. From another perspective, the actual physical process does depend on t_d because after departure the solid temperature field will rise again. An estimate for t_d can be obtained, for example, from the balance of the buoyancy force with the growth force as discussed in ref. [22]. In estimating t_d and calculating the growth force, the bubble growth rate, which is the solution to be sought here, is needed. This dilemma can be easily solved since we do not need the exact value of t_d in equations (24) and (26), and the growth rate can be estimated by using the constant wall temperature solution for $R(t)$ given by equation (18). Hence the estimate used here for t_d is

$$t_d\sim\left[\frac{c^2}{f^2(c)}\frac{Ja}{c_1Pr_l^{1/2}}\frac{\alpha_l^{1/2}}{g}\right]^{2/3} \tag{28}$$

which gives

$$Fo=\frac{\alpha_s\alpha_l^{1/3}}{g^{2/3}H^2}\frac{Ja^{2/3}}{c_1^{2/3}Pr_l^{1/3}}\frac{c^{4/3}}{f^{4/3}(c)}. \tag{29}$$

It is noted that the above choice for t_d is adopted.

Non-dimensionalization of the boundary condition on the liquid–solid interface, equation (14b), results in

$$\frac{\partial\theta_l}{\partial\bar{z}_l}=\frac{k_s}{k_l}\frac{L(\bar{r})}{H}\frac{\partial\theta_s}{\partial\bar{z}_s}.$$

Using

$$L(\bar{r})=\phi r,\ r=cR(t)\bar{r}=R_c(t_d)\,c\frac{R(t)}{R_c(t_d)}\bar{r},$$

equation (5a) for ϕ, and equation (18) for $R_c(t)$, the above can be expressed as

$$\frac{\partial\theta_l}{\partial\bar{z}_l}=\frac{\alpha^{1/2}}{\kappa}Fo^{1/2}\,c_1Pr_l^{1/2}\,\bar{R}(\tau)\bar{r}\frac{\partial\theta_s}{\partial\bar{z}_s}\quad\text{at }\bar{z}_s=0 \tag{30}$$

where the liquid-to-solid conductivity ratio and thermal diffusivity ratio,

$$\kappa=k_l/k_s \tag{31}$$

and

$$\alpha=\alpha_l/\alpha_s \tag{32}$$

are two more independent dimensionless parameters that are important to the bubble growth process in addition to Ja, Pr_l and Fo. It is noted that κ only appears in the boundary condition given by equation (30) while α appears in both the boundary condition

and the energy equation for the solid. Hence, the effect of α on the growth rate and the solid thermal field is more complicated than that of κ.

2.2.2. *Coordinate transformations.* To apply the boundary condition at large $\bar{r}$ for the solid temperature, the following simple transformations are applied in the $\bar{r}$-direction:

$$\bar{r} = \bar{r}_\infty \{1 - S_r \tan^{-1}[(1-\eta)\tan(1/S_r)]\} \quad \text{for } 0 \leqslant \eta \leqslant 1 \tag{33}$$

where $\bar{r}_\infty$ is the radial position at which equation (12b) is applied and the constant S_r determines the percentage of the grid number allocated to the region of $\bar{r} \leqslant 1$. Typically, $S_r = 0.7$–0.8 is used and $\bar{r}_\infty$ ranges from 5 to 25. To place more grids near $\bar{z}_s = 0$ where a large temperature gradient occurs, the following transformation is applied:

$$\bar{z}_s = -1 + S_z \tan^{-1}[(1-\zeta)\tan(1/S_z)] \quad \text{for } 0 \leqslant \zeta \leqslant 1 \tag{34}$$

where S_z is a constant characterizing the stretching. The clustering of the grids occurs near $\bar{z}_s = 0$. For a thicker plate, $S_z = 0.65$ is typically used. For a thin solid layer, a larger value of $S_z = 1.0$ is preferred because the thermal layer will quickly penetrate to the bottom soon after incipience.

The computation must start from some very small but nonzero initial time, τ_0, with the present formulation. Because the error for $\bar{R}(\tau)$ associated with τ_0 is of $O((\tau_0)^{1/2})$, it is desirable to use τ_0 as small as possible. To this end, the following transformation is introduced:

$$\tau = \sigma^2 \tag{35}$$

with a uniform "time step" $\Delta\sigma$.

The energy equation for the solid heater is transformed to (η, ζ) coordinates. The equation is

$$\frac{1}{2\sigma}\frac{\partial\theta_s}{\partial\sigma} - \frac{\bar{R}'(\tau)}{\bar{R}(\tau)}\bar{r}\frac{\partial\theta_s}{\partial\eta}\frac{\partial\eta}{\partial\bar{r}} = \frac{1}{\alpha}\frac{f^2(c)c_1^2 Pr_l}{c^6 Ja^2}\frac{1}{\bar{R}^2(\tau)}\frac{1}{\bar{r}}\frac{\partial}{\partial\eta}\left(\bar{r}\frac{\partial\theta_s}{\partial\eta}\frac{\partial\eta}{\partial\bar{r}}\right)\frac{\partial\eta}{\partial\bar{r}} + Fo\frac{\partial}{\partial\zeta}\left(\frac{\partial\theta_s\partial\zeta}{\partial\zeta\partial\bar{z}_s}\right)\frac{\partial\zeta}{\partial\bar{z}_s} + \frac{\alpha_s t_d q'''}{k_s \Delta T_{sat0}}. \tag{36}$$

It is solved using the ADI method [32] while that for the microlayer is solved by marching from $\bar{r} = 1$ to $\bar{r} = 0$.

2.2.3. *Solution procedure.* Due to the coupling between the solid and liquid temperature fields through the boundary conditions, θ_s and θ_l must be solved simultaneously at a given instant. However, θ_l needs to be solved only for $\bar{r} \leqslant 1$ while θ_s should be solved for $\bar{r} \leqslant \bar{r}_\infty$ with $\bar{r}_\infty \gg 1$. Hence, an iterative solution procedure is adopted which is briefly described.

The solutions for θ_s and θ_l are assumed to be known at $\sigma = \sigma^n$ as θ_s^n and θ_l^n. At $\sigma = \sigma^{n+1} = \sigma^n + \Delta\sigma$, the first iteration for θ_s^{n+1} is solved using the ADI scheme by simply marching in time by one time step for the given boundary condition $\theta_s^n(\bar{z}_s = 0)$. The liquid temperature θ_l is solved next with $\theta_s^n(\bar{z}_s = 0)$. After one sweep, the interface temperature $\theta_s^{n+1}(\bar{z}_s = 0)$ is updated by forcing the continuity of the heat flux,

$$\frac{\partial\theta_l}{\partial\bar{z}} = \frac{k_s}{k_l}\frac{\partial\theta_s}{\partial\bar{z}}.$$

The second iteration for θ_s^{n+1} begins with this updated condition at $\bar{z}_s = 0$. Several iterations bring the successive difference in temperature on the interface down to 10^{-3} (this tolerance is sufficient for the present computation). After the temperature fields converge at σ^{n+1} (or τ^{n+1}) the growth rate $\bar{R}(\tau^{n+1})$ is updated by integrating equation (22) using Euler's explicit scheme. The information for $\bar{R}(\tau^{n+1})$ is a necessary input in equations (24) and (26). Although the solution for $\bar{R}(\tau^{n+1})$ is only first order accurate in $\Delta\sigma$, the $O(\Delta\sigma)$ accuracy is not a concern here because a very small $\Delta\sigma$ has to be used to retain the numerical stability in solving the coupled equations (22), (24) and (26). Typically, $n = 10^4$ is needed for $\tau \leqslant 1$ to achieve the convergence of the solution with a moderate and large Ja if 16–26 grids are allocated in $0 \leqslant \bar{r} \leqslant 1$. For $Ja \sim 1$, the total number of time steps is on the order of $n = 8 \times 10^4$ for $Fo = 10$, 100 and 1000.

3. RESULTS AND DISCUSSIONS

3.1. *Determination of the empirical constants* c *and* c_l

After examining a limited number of photographs for growing vapor bubbles in saturated pool boiling [12, 14, 28] the following trend is observed:

(a) For high Jacob number, the bubble shape tends to resemble a hemisphere on top of a wedge (microlayer). Thus c is close to 1.

(b) For low Jacob number, the bubble shape is more spherical and c is thus small.

The values of c are determined from the vapor bubble profiles and the photographs provided by Van Stralen and Cole [12], Akiyama *et al.* [14] and Hospeti and Mesler [28]. The following correlation for c best fits those data:

$$c = [(0.4134 Ja^{0.1655})^{-6} + (1 - 0.1e^{-0.0005Ja})^{-6}]^{-1/6}. \tag{37}$$

Figure 2 compares the above fit with the data. It is possible that c may also depend on other parameters such as Pr_l and Fo. For the purpose of developing a model for predicting the bubble growth rate, a simple form for c is adopted and c_l is allowed to vary with Ja, Pr_l and α. As will be demonstrated, this approach turns out to be quite useful.

The determination of c_l, which describes the microlayer wedge angle as shown by equation (5), is crucial to the success of the present study. Because the hydrodynamics are not considered in this analysis, c_l must

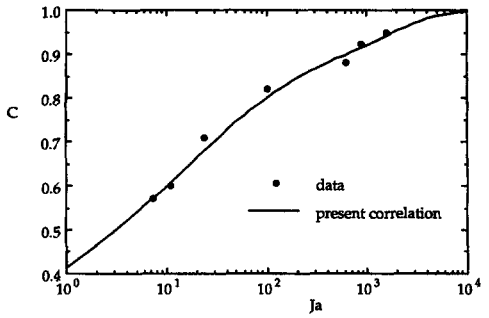

Fig. 2. Dependence of c on Ja based on the data of refs. [12], [14] and [27].

be determined empirically. For each experimentally measured $R(t)$, a series of values for c_1 are used in the numerical computation for θ_s, θ_l and $R(t)$. The one that results in the closest agreement between the measured and computed $R(t)$ over a large range of t prior to departure is taken to be the value of c_1 required in the present analysis. The results of such are given in Table 1. The data are presented from large Ja to small Ja. Based on these 32 data sets, the following correlation for c_1 is obtained:

$$c_1 \sim 0.00643 Ja^{0.763} Pr_l^{-0.390} \kappa^{0.0746} \alpha^{-0.221}$$

by requiring the least relative deviation

$$\mathrm{rd} = \frac{1}{32} \sum_{n=1}^{32} |c_{1n} - c_{1n}^*| / c_{1n}^*,$$

in which c_1^* is the value determined from matching the experimental growth rate data with the present computation. The above expression gives rd = 0.232. A very similar expression is obtained with a standard deviation of 0.19 for the exponent of Pr_l using a least squares fitting. Hence, within statistical error, the exponent for Pr_l may be taken as -0.5. Requiring the least relative deviation again,

$$c_1 Pr_l^{1/2} \sim 0.00525 Ja^{0.752} \kappa^{-0.113} \alpha^{-0.117} \quad (38)$$

with a relative deviation of 0.238. Figure 3 compares the above correlation for c_1 with the data presented in Table 1; reasonable agreement is observed. An important implication immediately follows when one substitutes equation (38) into equations (5a), (18), (24) and (26)–(30) which are the only places where Pr_l appears. Since c_1 and Pr_l appear in the form of $c_1 Pr_l^{1/2}$, it is obvious that Pr_l is no longer relevant to the present problem. This implies that the liquid viscosity is not important in determining the bubble shapes which are characterized by c and c_1 in the present analysis.

To understand the independence of vapor bubble shape on the liquid viscosity, it is instructive to esti-

Table 1. Microlayer angle parameter c_1 determined from various sources

No.	Ja	Pr_l	K_l/K_s	α_l/α_s	c_1	P (atm)	Source
1	1973.6	4.65	0.00156	0.00126	3.10	0.040	Van Stralen *et al.* [12]
2	887.3	4.22	0.00161	0.00130	1.75	0.079	Van Stralen *et al.* [12]
3	766.2	4.54	0.0270	0.01210	1.30	0.066	Cole and Shulman [11]
4	389.5	3.46	0.00164	0.00133	1.20	0.132	Van Stralen *et al.* [12]
5	289.3	3.42	0.02840	0.01260	0.65	0.129	Cole and Shulman [11]
6	210.0	6.44	0.00577	0.00810	0.33	0.063	Cole and Shulman [11]
7	201.0	2.97	0.00166	0.00136	0.47	0.203	Van Stralen *et al.* [12]
8	178.7	2.76	0.0290	0.01290	0.55	0.257	Cole and Shulman [11]
9	156.0	6.70	0.00449	0.00604	0.30	0.182	Cole and Shulman [11]
10	150.5	2.70	0.00168	0.00137	0.45	0.267	Van Stralen *et al.* [12]
11	130.0	6.13	0.00870	0.00830	0.25	0.268	Cole and Shulman [11]
12	90.6	2.17	0.02970	0.01331	0.20	0.474	Cole and Shulman [11]
13	67.1	5.60	0.00860	0.00815	0.17	0.40	Cole and Shulman [11]
14	50.6	4.74	0.00508	0.00629	0.30	0.689	Cole and Shulman [11]
15	50.0	5.14	0.00848	0.00808	0.16	0.522	Cole and Shulman [11]
16	42.3	1.76	0.00173	0.00144	0.52	1.0	Staniszewski [13]
17	37.6	4.60	0.00837	0.00806	0.15	0.711	Cole and Shulman [11]
18	35.8	1.76	0.00173	0.00144	0.38	1.0	Staniszewski [13]
19	25.3	1.76	0.00173	0.00144	0.25	1.0	Staniszewski [13]
20	25.0	1.76	0.00173	0.00144	0.30	1.0	Staniszewski [13]
21	24.5	4.25	0.00493	0.00597	0.10	1.0	Cole and Shulman [11]
22	23.4	1.76	0.00730	0.00577	0.12	1.0	Hospeti and Mesler [27]
23	23.0	4.30	0.00048	0.00086	0.18	1.0	Staniszewski [13]
24	18.8	1.76	0.00730	0.00577	0.10	1.0	Hospeti and Mesler [27]
25	18.4	1.76	0.00173	0.00144	0.28	1.0	Keshock and Siegel [15]
26	14.9	1.76	0.00730	0.00577	0.07	1.0	Hospeti and Mesler [27]
27	11.5	1.43	0.02630	0.02440	0.06	2.0	Akiyama *et al.* [14]
28	11.2	1.44	0.00174	0.00146	0.20	1.90	Staniszewski [13]
29	9.16	1.30	0.00175	0.00148	0.16	2.72	Staniszewski [13]
30	7.73	4.0	0.00046	0.00068	0.050	1.90	Staniszewski [13]
31	1.17	1.02	0.02620	0.02470	0.015	8.0	Akiyama *et al.* [14]
32	0.52	0.92	0.02560	0.02430	0.007	15.0	Akiyama *et al.* [14]

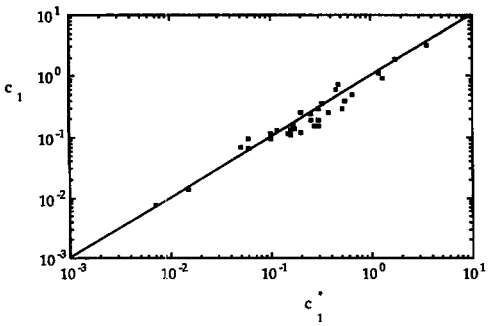

Fig. 3. Comparison for c_1 based on the correlation and data.

mate the Reynolds number of the liquid motion associated with the bubble growth. Using $d = 2R(t)$ as the length scale, $\dot{R}(t)$ as the velocity scale, assuming $R(t) \sim \beta t^{1/2}$, the Reynolds number of the liquid flow may be estimated as $Re_d \sim \beta^2/\nu_l$. For case No. 3 ($Ja = 766.2$) listed in Table 1, using the measured growth rate shown in Fig. 4(b), it is easily shown that $Re_d \sim 12,941$ for $\beta^2 \sim 8.8$ (mm^2 ms^{-1}) and $\nu_l = 6.8 \times 10^{-3}$ (cm^2 s^{-1}). Hence, the liquid motion induced by the expanding bubble in this case is clearly of inviscid nature. Even for case No. 28 ($Ja = 11.2$) for which $\beta^2 \sim 0.064$ (mm^2 ms^{-1}), one obtains $Re_d \sim 256$ by taking $\nu_l = 5 \times 10^{-3}$ (cm^2 s^{-1}). Typically, $Re_d \sim 40$ may be the lower limit above which a uniform liquid flow around a bubble can be treated as inviscid flow. For the present case, the bulk liquid motion is mainly in the radial direction. Because the viscous effect associated with the radial motion is weaker than that in a uniform flow over a sphere, the liquid flow induced by the growing bubble in the present study is mainly of inviscid nature. Therefore the hydrodynamics, which is important to the bubble shape appears to have a universal effect on the bubble growth rate, i.e. independent of the liquid viscosity, for most of the data listed in Table 1. The foregoing discussion also, to certain extent, justifies the choice of using Ja alone to correlate c as given by equation (37).

3.2. *Comparison of the predicted and measured growth rate*

To validate the present numerical analysis and also to examine the effect of the Jacob number, Ja, on the growth rate, comparisons are made between the present prediction and the experimentally measured $R(t)$ over a large range of Ja. Figure 4(a) shows such a comparison in the high Jacob number range, $Ja = 201$–1973.6 at $\kappa = 0.00156$–0.0016. The data are taken from Van Stralen *et al.* [12] who used water as the boiling liquid. The Prandtl number, Pr_l, in Fig. 4(a) changes from 2.97 to 4.65; but it is not expected that Pr_l will affect the growth rate. Excellent agreement is observed between the prediction and the measurement in this large Ja range. Figure 4(b) compares the numerical results with the data of Cole and Shulman [11] in which Ja ranges from 90.6 to 766.2, $\kappa = 0.027$–0.0297 and $Pr_l = 2.17$–4.54. For these intermediate to high values of Ja, excellent agreement for $R(t)$ is again observed. Figure 4(c) compares the prediction with the data obtained by Cole and Shulman [11] using methanol as the boiling liquid which has a higher Prandtl number, $Pr_l = 4.6$–6.13. The Jacob number ranges from 37.6 to 130.0 which is considered to be in the intermediate range. Very good agreement is seen between the data and the prediction. While the measurements shown in Figs. 4(a)–(c) were obtained under subatmospheric or atmospheric conditions, Fig. 4(d) compares the present prediction with the data of Staniszewski [13] obtained at $p_{sat} = 193$ and 276 kpa (or 28 and 40 psi), respectively, with $Ja = 11.2$ and 9.16. Even at this elevated pressure with relatively low Jacob number, good agreement can still be observed for most of the time. From Figs. 4(a)–(d), it is very obvious that $R(t)$ strongly depends on Ja; an increasing Ja results in an increasing growth rate—a well-established fact.

It is also noted that, at 276 kpa pressure, the present model over-predicts $R(t)$ at the later stage of growth. The data (No. 31 and No. 32 in Table 1) by Akiyama *et al.* [14] were obtained at even higher pressure. For those two cases the Reynolds number is of $O(1)$, especially at the later stage of growth. Hence, detailed hydrodynamics may need to be properly accounted for in order to improve the prediction. Another source of the error for $R(t)$ at low Jacob number may be associated with equation (4) in which the energy transfer at the vapor dome between the bubble and the bulk liquid is neglected based on the assumption that the bulk liquid is at saturated conditions. This would only cause a small error if $R(t)$ is much larger than the thermal layer thickness, δ_{th}, of the bulk liquid for most of the growth period. At low Ja, the bubble is typically small and, hence, the bubble growth may occur largely within the thermal layer. Under such conditions, the unsteady heat transfer between the vapor dome and the bulk liquid is no longer negligible. From this view point, the present analysis may not be directly applied to very low Jacob number boiling systems without further study.

4. CONCLUSIONS

In Part I of the present study, a numerical analysis is formulated to study the growth of vapor bubbles in saturated heterogeneous boiling. The thermal interaction of the temperature fields in the thin liquid microlayer and in the solid heater must be properly accounted for in order to accurately predict the growth rate of vapor bubbles attached to a heating surface. The vapor bubble shape parameter, c, and the microlayer wedge angle parameter, c_1, are two empirically determined constants which are used in the numerical computation. In particular, the wedge angle parameter, c_1, is obtained by matching the measured and predicted bubble growth rate. It is important to note that once c_1 is correctly specified in

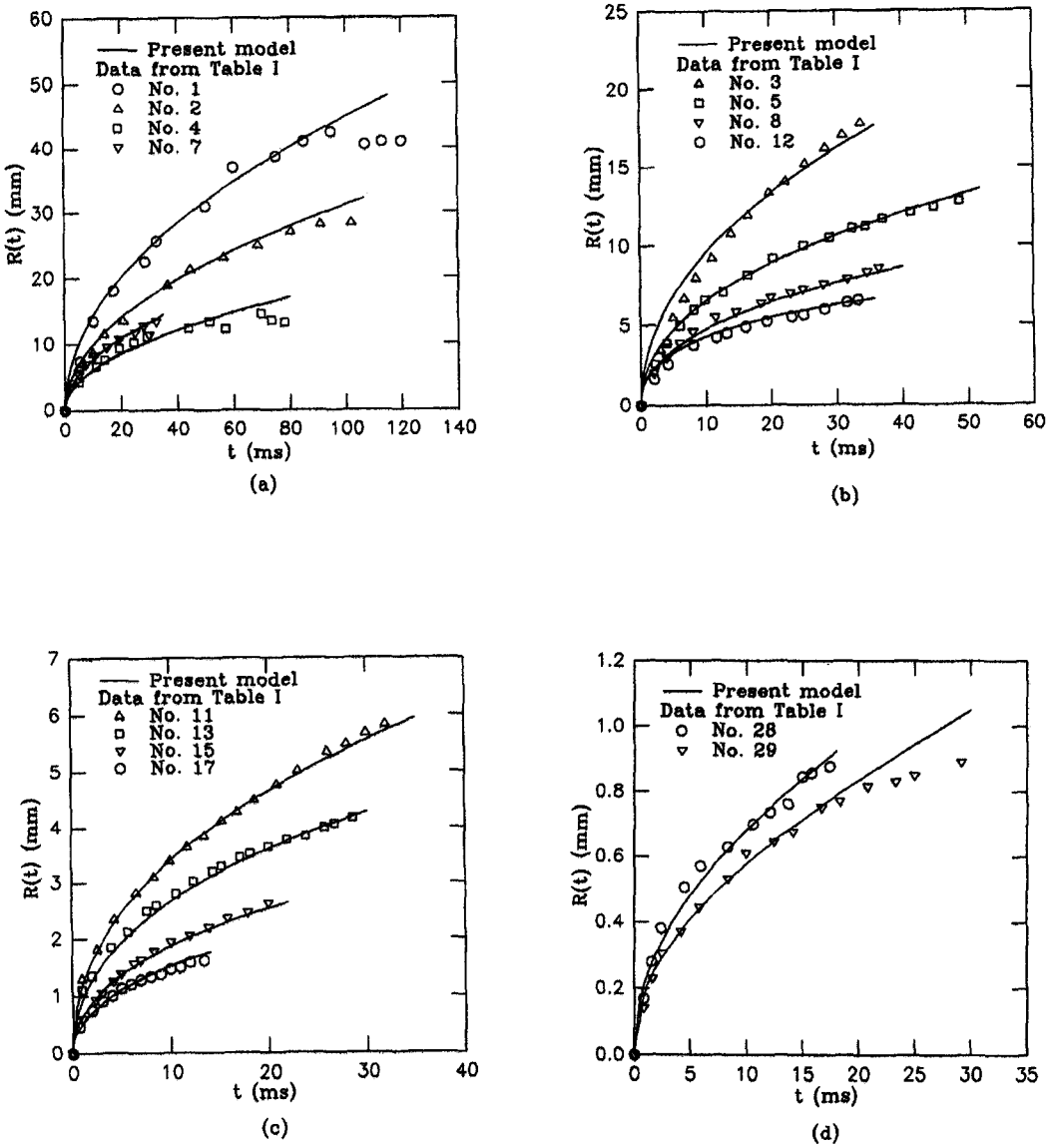

Fig. 4. Comparison of the bubble growth rate $R(t)$ between the present numerical prediction and various data: (a) comparison with the data of Van Stralen *et al.* [12] using water as boiling liquid; (b) comparison with the data of Cole and Shulman [11] using water as boiling liquid; (c) comparison with the data of Cole and Shulman [11] using methanol as boiling liquid and (d) comparison with the data of Staniszewski [13] using water as boiling liquid at elevated pressure.

the computation, the predicted bubble growth rate compares very well with the reported experimental data over a wide range of conditions during the entire growth period. The empirically determined correlation for c_1 suggests that the liquid Prandtl number, and hence the viscosity of the liquid, plays little role in the bubble growth process. A subsequent estimate indicates that the Reynolds number of the bulk liquid motion induced by the bubble is of inviscid nature; thus the viscosity is not important in determining the parameters c and c_1.

The dimensional analysis for the governing equations and boundary conditions shows that there exist four relevant dimensionless parameters for bubble growth: Jacob number Ja, Fourier number Fo of the solid based on the thickness of the heater and the bubble departure time scale, the liquid-to-solid conductivity ratio κ, and the liquid-to-solid thermal diffusivity ratio α. The Jacob number is the most important one affecting c, c_1, and dimensionless growth rate $\bar{R}(\tau)$. The effects of the four parameters on $\bar{R}(\tau)$ and the thermal fields of the liquid and the solid heater will be discussed in Part II of the present study [29].

REFERENCES

1. P. Dergarabedian, The rate of growth of vapour bubbles in superheated water, *J. Appl. Mech.* **20**, 537–545 (1953).

2. M. S. Plesset and S. A. Zwick, The growth of vapour bubbles in superheated liquids, *J. Appl. Phys.* **25,** 493–500 (1954).
3. H. K. Forster and N. Zuber, Growth of a vapour bubble in a superheated liquid, *J. Appl. Phys.* **25,** 474–478 (1954).
4. L. E. Scriven, On the dynamics of phase growth, *Chem. Engng Sci.* **10,** 1–13 (1959).
5. P. Griffith, Bubble growth rates in boiling, *ASME Trans.* **80,** 721–727 (1958).
6. N. Zuber, The dynamics of vapor bubbles in nonuniform temperature fields, *Int. J. Heat Mass Transfer* **2,** 83–98 (1961).
7. L. A. Skinner and S. G. Bankoff, Dynamics of vapor bubbles in spherically symmetric temperature fields of general variation, *Physics Fluids* **7,** 1–6 (1964).
8. C. Y. Han and P. Griffith, The mechanism of heat transfer in nucleate pool boiling—I. Bubble initiation, growth and departure, *Int. J. Heat Mass Transfer* **8,** 887–904 (1965).
9. S. J. D. Van Stralen, The mechanism of nucleate boiling in pure liquids and in binary mixtures—I–IV, *Int. J. Heat Mass Transfer* **9,** 995–1020, 1021–1046 (1966); **10,** 1469–1484, 1485–1498 (1967).
10. B. B. Mikic, W. M. Rohsenow and P. Griffith, On bubble growth rates, *Int. J. Heat Mass Transfer* **13,** 657–666 (1970).
11. R. Cole and H. L. Shulman, Bubble growth rates at high Jacob numbers, *Int. J. Heat Mass Transfer* **9,** 1377–1390 (1966).
12. S. J. D. Van Stralen, R. Cole, W. M. Sluyter and M. S. Sohal, Bubble growth rates in nucleate boiling of water at subatmospheric pressures, *Int. J. Heat Mass Transfer* **18,** 655–669 (1975).
13. B. E. Staniszewski, Bubble growth and departure in nucleate boiling, Tech. Rept. No. 16, MIT, Cambridge, MA (1959).
14. M. Akiyama, F. Tachibana and N. Ogawa, Effect of pressure on bubble growth in pool boiling, *Bull. JSME* **12,**(53), 1121–1128 (1969).
15. E. G. Keshock and R. Siegel, Forces acting on bubbles in nucleate boiling under normal and reduced gravity conditions, NASA Tech. Note TN D-2299 (1964).
16. D. A. Labunstov, Mechanism of vapour bubble growth in boiling on the heating surface, *J. Engng Phys.* **6**(4), 33–39 (1963).
17. M. G. Cooper, The microlayer and bubble growth in nucleate pool boiling, *Int. J. Heat Mass Transfer* **12,** 915–933 (1969).
18. G. S. Dzakowic and W. Frost, Vapour bubble growth in saturated pool boiling by microlayer evaporation of liquid at the heated surface, *Proceedings of the 4th International Heat Transfer Conference*, Paris, Vol. 5, paper B2.2. Elsevier, Amsterdam (1970).
19. N. S. Srinivas and R. Kumar, Prediction of bubble growth rates and departure volumes in nucleate boiling at isolated sites, *Int. J. Heat Mass Transfer* **27,** 1403–1409 (1984).
20. M. G. Cooper and R. M. Vijuk, Bubble growth in nucleate pool boiling, *Proceedings of the 4th International Heat Transfer Conference*, Paris, Vol. 5, paper B2.1. Elsevier, Amsterdam (1970).
21. S. J. D. Van Stralen, M. S. Sohal, R. Cole and W. M. Sluyter, Bubble growth rates in pure and binary systems: combined effect of relaxation and evaporation microlayers, *Int. J. Heat Mass Transfer* **18,** 453–467 (1975).
22. M. V. Fyodorov and V. V. Klimenko, Vapour bubble growth in boiling under quasi-stationary heat transfer conditions in a heating wall, *Int. J. Heat Mass Transfer* **32,** 227–242 (1989).
23. R. C. Lee and J. E. Nydahl, Numerical calculation of bubble growth in nucleate boiling from inception through departure, *J. Heat Transfer, Trans. ASME* **111,** 474–479 (1989).
24. L. Z. Zeng, J. F. Klausner and R. Mei, A unified model for the prediction of bubble detachment diameters in boiling systems—I. Pool boiling, *Int. J. Heat Mass Transfer* **36,** 2261–2270 (1993).
25. L. Z. Zeng, J. F. Klausner, D. M. Bernhard and R. Mei, A unified model for the prediction of bubble detachment diameters in boiling systems—II. Flow boiling, *Int. J. Heat Mass Transfer* **36,** 2271–2279, (1993).
26. J. W. Westwater, Things we don't know about boiling heat transfer. In *Research in Heat Transfer*, pp. 61–73. Pergamon Press, New York (1963).
27. F. M. Moore and R. B. Mesler, The measurement of rapid surface temperature fluctuations during nucleate boiling of water, *A.I.Ch.E. Jl* 7(4), 620–624 (1961).
28. N. B. Hospeti and R. B. Mesler, Vaporization at the base of bubbles of different shape during nucleate boiling of water, *A.I.Ch.E. Jl* **15**(2), 214–219 (1969).
29. R. Mei, W. Chen and J. F. Klausner, Vapor bubble growth in heterogeneous boiling—II. Growth rate and thermal fields, *Int. J. Heat Mass Transfer* **38,** 921–934 (1995).
30. L. D. Koffman and M. S. Plesset, Experimental observations of the microlayer in vapor bubble growth on a heated solid, *J. Heat Transfer, Trans. ASME* **105,** 625–632 (1983).
31. M. G. Cooper and A. J. P. Lloyd, The microlayer in nucleate pool boiling, *Int. J. Heat Mass Transfer* **12,** 895–913 (1969).
32. D. A. Anderson, J. C. Tennehill and R. H. Pletcher, *Computational Fluid Mechanics and Heat Transfer*, p. 549. McGraw-Hill, New York (1984).